



HAL
open science

A metamodel for confined yield stress flows and parameters' estimation

Clément Berger, David Coulette, Paul Vigneaux

► **To cite this version:**

Clément Berger, David Coulette, Paul Vigneaux. A metamodel for confined yield stress flows and parameters' estimation. *Rheologica Acta*, 2024, 10.1007/s00397-024-01436-0 . hal-04480999

HAL Id: hal-04480999

<https://hal.science/hal-04480999>

Submitted on 27 Feb 2024

HAL is a multi-disciplinary open access archive for the deposit and dissemination of scientific research documents, whether they are published or not. The documents may come from teaching and research institutions in France or abroad, or from public or private research centers.

L'archive ouverte pluridisciplinaire **HAL**, est destinée au dépôt et à la diffusion de documents scientifiques de niveau recherche, publiés ou non, émanant des établissements d'enseignement et de recherche français ou étrangers, des laboratoires publics ou privés.



Distributed under a Creative Commons Attribution 4.0 International License

A metamodel for confined yield stress flows and parameters' estimation^{*}

Clément Berger^{a,1}, David Coulette^{a,2} and Paul Vigneaux^{a,b,*,2}

^aUMPA CNRS UMR 5669 ENS de Lyon, 46 Allée d'Italie, Lyon, 69364, Rhône, France

^bLAMFA CNRS UMR 7352 Université de Picardie Jules Verne, 33 Rue Saint Leu, Amiens, 80039, Somme, France

ARTICLE INFO

Keywords:

Herschel-Bulkley
lubrication approximation
closed domain
inverse problem
Polynomial Chaos Expansion
Principal Component Analysis

ABSTRACT

With the growing demand of mineral consumption, the management of the mining waste is crucial. Cemented paste backfill (CPB) is one of the techniques developed by the mining industry to fill the voids generated by the excavation of underground spaces. The CPB process is the subject of various studies aimed at optimizing its implementation in the field. In this article, we focus on the modelling of the backfill phase where it has been shown in [Vigneaux et al., Cem. Concr. Res. 164 (2023) 107038] that a viscoplastic lubrication model can be used to describe CPB experiments. The aim here is to propose an accelerated method for performing the parameters' estimation of the properties of the paste (typically its rheological properties), with an inverse problem procedure based on observed height profiles of the paste. The inversion procedure is based on a metamodel built from an initial partial differential equation model, thanks to a Polynomial Chaos Expansion coupled with a Principal Component Analysis.

1. Introduction

In this article, we focus on a fast model for the simulation and parameters' estimation of thin sheets of viscoplastic material aiming at filling elongated cavities. A typical application would be the cemented paste backfill in underground stopes.

With the growing demand of mineral consumption, the management of the mining waste is crucial. Cemented paste backfill (CPB) is one of the techniques developed by the mining industry to fill the voids generated by the excavation of underground spaces. CPB has been documented in Germany in the 1980's Landriault (2006). It is now used in a growing number of countries across the world, including Australia, Canada and China Yilmaz and Fall (2017). The paste is obtained by mixing tailings coming from the extraction, with water and a hydraulic binder. Mixtures are then transported from the surface plant to the underground openings through pipes. Addition of the binder (cement like) is crucial for the final strength and stability of the backfill. Among the advantages of the CPB, one expects:

- the ability of reusing the mining waste by reintroducing it in the mine. This would prevent to use surface spaces on the ground (e.g., tailings dams), with all the potential environmental impacts this can have (UNCED (1992) and Azam and Li (2010)).


- By filling the voids in underground spaces with these pastes, the ground is thus consolidated, leading to two advantages: (i) the risk of subsidence Keller (2008) is lowered and (ii) there is no need to leave unexploited pillars as done originally for stability, since the whole cavity can then be backfilled with the cemented paste (like in the cut-and-fill mining methodology). A better exploitation of the mining deposit can thus be expected.

The practical implementation of CPB is a complex process where optimization needs to be done on several aspects: the composition of the CPB (chemical and mineralogical characteristics) and its resulting physical properties in relation with the transportation phase (where fluidity would ease the pumping) and finally the consolidating phase (where high mechanical strength is needed for an efficient stability of the resulting backfilled volume) Yilmaz and Fall (2017).

In the present paper, we focus more specifically on the modelling and simulation of the filling phase where we consider the slurry of a viscoplastic material in a *bounded domain*. We refer to Vigneaux et al. (2023) for a more detailed description on the modelling where it was shown that a viscoplastic lubrication model successfully described laboratory experiments of such slurries made of typical CPB material. Using this model, we present here a new methodology to perform parameters' estimation of this model thanks to an inverse problem using *observations* of the surface height of the slurry. The objective of the present article is thus to provide a fast algorithm which allows to simulate an observed paste flow and to determine its viscoplastic properties, typically the viscosity (or consistency), the yield stress and the power index of the constitutive law of the associated rheology (namely, the Herschel-Bulkley law). As a matter of fact the rheology is one of the most important properties of CPB material Yilmaz and Fall (2017); Roussel and Coussot (2005). Having these parameters, we can then

^{*}Supplementary code on Zenodo, ref 8377205. This is the authors' version as of: February 23, 2024. Now accepted in: Rheologica Acta (2024) <https://doi.org/10.1007/s00397-024-01436-0>

^{*}Corresponding author

 clement.berger@ens-lyon.fr (C. Berger);

david.coulette@ens-lyon.fr (D. Coulette); paul.vigneaux@math.cnrs.fr (P. Vigneaux)

ORCID(s): 0009-0003-0055-0803 (C. Berger); 0000-0002-3556-0089 (D. Coulette); 0000-0001-6606-5446 (P. Vigneaux)

¹Funded by a CDSN grant from the French MESRI

²Funded by the French ANR under grant number ANR-20-CE46-0006

solve the direct problem to simulate further in time and optimize the filling process of the cavity.

To perform the inverse problem in a faster way, we develop a so called *metamodel* which is a *precise* approximation of the lubrication model (in its original partial differential equation (PDE) form) but *much faster* to evaluate than solving the PDE. (Metamodels are also sometimes called *surrogate* models.) Indeed, when considering the closed stope configuration, there is no explicit solution for the height profile and a numerical resolution is required. The design of this algorithm borrows from previous works Blatman and Sudret (2013); Hawchar et al. (2017) but seems to have been rarely adapted in the context of PDEs. We develop here a specific and complete framework for the model of Vigneaux et al. (2023). Of note, we also provide in an open access repository the data and code of the metamodel¹, so that readers can experiment and identify the parameters of their own CPB lab experiments.

The paper is organized as follows. In section 2, we detail the model under consideration and the numerical resolution of the direct problem, as well as the links with the inverse problem. We then present in section 3 the construction of the metamodel, which mixes Polynomial Chaos Expansion (PCE) and a Principal Component Analysis (PCA). In section 4, we test the metamodel performances depending on the characteristics of the PCA and the PCE. We also measure the ability to estimate the parameters when the metamodel is coupled to a Nelder-Mead algorithm to solve the inverse problem for both synthetic data (*in silico*) or for the laboratory experiments data of Vigneaux et al. (2023).

2. Formulation of the direct problem

2.1. Original PDE model

The starting model is a so-called lubrication model for yield stress flows in confined geometry. It is borrowed from Balmforth et al. (2006) developed in unconfined geometry (see also earlier works Liu and Mei (1989); Coussot et al. (1996); Huang and Garcia (1998)). It was then studied in the case of the flow in a confined cavity by Vigneaux et al. (2023). We refer to Balmforth et al. (2006) and Vigneaux et al. (2023) for more details.

We consider a closed cavity in 1D, inclined at an angle ϕ to the horizontal (see figure 1). In non-dimensional variables the length of this cavity is equal to 1. We assume that the material follows a Herschel-Bulkley constitutive law (whose characteristic parameters: yield stress, consistency and power index will be described later). It is assumed that the injected flow rate of the material is imposed on the left of the domain. The non-dimensionalization process leads to $q = 1$ as the left boundary condition for the model at $x = 0$. While on the right, at $x = 1$, a wall condition is imposed with $q = 0$. The unknown of the problem that is solved is the dimensionless height h of the material at time t and distance x from the injection point. Note that we assume that there is no material at $t = 0$ (the cavity is empty), so that the initial

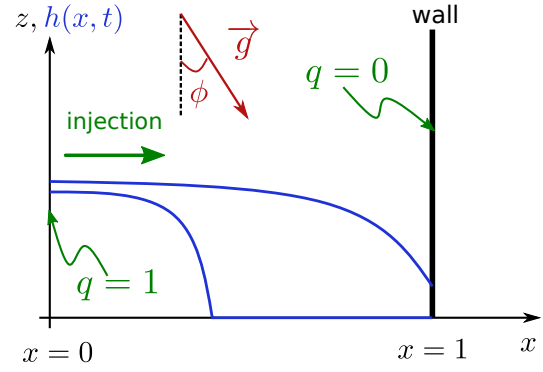


Figure 1: 1D model, non-dimensionalized variables. The blue curve is the height h of the material at two successive times (the flow is from left to right). Note that the gravity vector is inclined with an angle ϕ since the x axis is assumed to be inclined downslope from the horizontal.

condition of the PDE is : $h(x, t = 0) = 0$ for all $x \in [0, 1]$. The evolution of h is the solution of the following partial differential equation (PDE):

$$\frac{\partial}{\partial t} h(x, t) + \frac{\partial}{\partial x} q(x, t) = 0, \forall x \in]0, 1[, \forall t > 0, \quad (1)$$

where $q(x, t)$ is the flux function defined as:

$$q(x, t) = \operatorname{sgn} \left(S - \frac{\partial h(x, t)}{\partial x} \right) \left| S - \frac{\partial h(x, t)}{\partial x} \right|^{1/n} \times \frac{nY(x, t)^{1+1/n}}{(n+1)(2n+1)} ((2n+1)h(x, t) - nY(x, t)), \quad (2)$$

where $\operatorname{sgn}(\cdot)$ is the sign function and n (dimensionless, typically in $[0.3; 1.2]$) is the power index of the aforementioned constitutive law. The variable $Y(x, t)$ encodes the yield surface (i.e., the height above which the material behaves like a pseudo-plug) and is given by:

$$Y(x, t) = \max \left(h(x, t) - \frac{B}{\left| S - \frac{\partial h}{\partial x}(x, t) \right|}, 0 \right), \quad (3)$$

where B is the Bingham number and S the so-called slope parameter, in this context.

Note that, as such, the independent parameters of this model are B , S and n . Knowing (B, S, n) , using aforementioned initial condition on h and boundary conditions on q , one can compute the evolution of h in the cavity. We now detail these parameters in terms of the associated dimensional variables. The slope parameter S is given by:

$$S = \frac{\tan \phi}{\epsilon}, \quad (4)$$

where $\epsilon = \hat{H}_0 / \hat{L}$ is the aspect ratio between the typical height of the material (\hat{H}_0 in m) and the typical length of the cavity (\hat{L} in m , in the x direction depicted in figure 1). In the lubrication theory (thin film), it is assumed that $\epsilon \ll 1$.

¹<https://zenodo.org/records/8377205>

The Bingham number is defined as:

$$B = \frac{\hat{H}_0 \hat{\tau}_y}{\hat{\rho} \hat{\nu} \hat{U}}, \quad (5)$$

where $\hat{\tau}_y$ ($kg.m^{-1}.s^{-2}$ or Pa) is the yield stress of the viscoplastic material, $\hat{\rho}$ is the density ($kg.m^{-3}$), \hat{U} is the characteristic downslope velocity ($m.s^{-1}$). The parameter $\hat{\nu}$ is the characteristic kinematic viscosity:

$$\hat{\nu} = \frac{\hat{\kappa}}{\hat{\rho}} \left(\frac{\hat{U}}{\hat{H}_0} \right)^{n-1}, \quad (6)$$

where $\hat{\kappa}$ ($kg.m^{-1}.s^{n-2}$ or $Pa.s^n$) is the consistency associated to the Herschel-Bulkley rheology.

The typical height of the cavity \hat{H}_0 can be computed through:

$$\hat{H}_0 = \left(\frac{\hat{\kappa} \hat{L}}{\hat{\rho} \hat{g} \cos \phi} \left(\frac{\hat{Q}_0}{\hat{W}} \right)^n \right)^{\frac{1}{2(1+n)}}, \quad (7)$$

where $\hat{g} = 9.81$ ($m^2.s^{-1}$) is the gravitational acceleration (note that $\hat{g} = \|\vec{g}\|$ of figure 1), \hat{W} (m) is the transverse width of the cavity and \hat{Q}_0 ($m^3.s^{-1}$) is the known injected flow rate of material. Note that if one starts from the given dimensional input data, one can begin with (7) and using:

$$\hat{U} = \frac{\hat{Q}_0}{\hat{W} \hat{H}_0} \quad (8)$$

one can compute subsequently the non dimensional quantities of the problem.

To fix the ideas, we recall the range of values for the parameters (B, S, n). In the context of CPB a "secured choice" (meaning extending a bit the range of potential extreme values) of values is $B \in [0.5, 250]$ and $S \in [\sim 0.1 \text{ or } 1, 120]$. Concerning the power law index, it is generally observed $n \approx 1$. More commonly, one might find CPB parameters of real mines close to $(B, S, n) \sim (150, 12, 1)$ (see Vigneaux et al. (2023) for more details). We will come back to this point at the end of the article.

2.2. Numerical solver

The solution of (1)-(2) is approximated by a numerical solver. It should be noted that this model has been extensively tested in various configurations by leading groups in the field Balmforth et al. (2006); Liu et al. (2016); Hogg and Matson (2009). So, even if it seems difficult to find a rigorous proof of the existence and uniqueness of this model in the literature, it does seem to be well-posed (in Hadamard's sense) in the configuration studied here. The time evolution is treated by an explicit scheme (forward Euler). The spatial discretization is treated using a centered scheme for $\partial h / \partial x$ and an upwind scheme for $\partial q / \partial x$. Using the boundary conditions, q can be computed for all the points

of the mesh, which enables to compute h for all points except the first one at $x = 0$ (which would require the evaluation of $q(-\Delta x)$). This point is treated by using the boundary condition $q(0) = 1$ and a downwind scheme for $\partial h / \partial x$. The resulting equation on $h(t, 0)$ cannot be computed in closed form (see (2)) and leads to a scalar non linear equation whose root can be solved with standard built-in libraries (e.g. `fzero` in Matlab or `brenth` in Python-Scipy). Cf. appendix A.1 for more details.

For a given spatial discretization (Δx) we adapt the time step (Δt) dynamically at each time iteration. A stability condition has been heuristically derived so that the time step is determined by the spatial step. This is done by taking the minimum of the two classical numerical stability constraints on Δt associated to the non-linear advection-diffusion problem (1)-(2). Namely, a constraint due to the advection component of (1) (CFL condition) and a constraint due to the explicit treatment of the diffusion component (Δt constrained by Δx^2) (LeVeque, 2004). Cf. appendix A.2 for more details. It should also be noted that there is no difficulty in dealing with the front where h vanishes, due to the nature of this PDE which includes the threshold (3).

To determine the spatial step, a numerical study of the convergence (Δx is refined, and therefore also Δt by the stability condition (33)) was performed. A reference solution has been computed beforehand using a very small Δx (with $n_x = 9601$ points in the mesh). Then, this solution is compared with the use of others bigger Δx ($n_x = 76, 151, 301, \dots, 4801$), to evaluate if there is a numerical convergence of the norm of the difference of the two solutions, as Δx is reduced. The comparison is done at a final meaningful time: the one at which the fluid has reached the right wall, a time referred to as *wall-touch*. An example of such study is illustrated on the figure 2 for $B = 100$, $S = 120$ and $n = 0.8$. We see that the numerical scheme is convergent with an exponent power of at least 0.6. This exponent is not very high, which is known to be associated to the stiffness of the non-linear problem. The development of higher order schemes is out of the scope of this paper. Note that we also perform the same kind of study for $(B = 30, S = 15, n = 0.8)$ and $(B = 70, S = 0.3, n = 0.8)$ which also show that the scheme is convergent with an order between 0.6 and 1. This validates the use of this whole solver.

Some (B, S) parameters lead to very fast resolutions, but some others can take up to two hours for $n_x = 301$ or multiple weeks for higher values of n_x . These correspond to high values of B and low values of S , i.e., a high yield stress and a low slope. For such parameters, the wall-touch happens at higher time so many more time steps have to be performed. As a compromise deduced from the above study, the use of $n_x = 301$ provides very good accuracy while leading to reasonable computation times, in the perspective of building a metamodel, as explained below.

This said, such numerical resolution remains costly, especially for some (B, S, n) parameters. Assume now that we want to use this solver to estimate the parameters (B, S, n) , given measured data of $h(x, t)$ profiles. We will then need

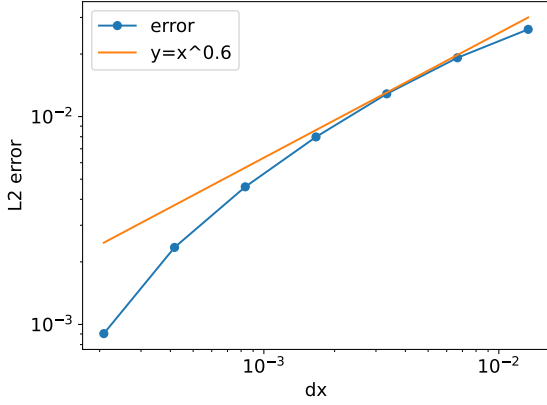


Figure 2: Study of the convergence (Δx is refined, and therefore also Δt by (33)) of the PDE numerical solver for $B = 100$, $S = 120$, $n = 0.8$. All solutions have been computed at their respective wall-touch time. The reference solution (h^{ref}) has been computed using $n_x = 9601$ points. The L^2 error ($\|h^{ref}(x) - h^{\Delta x, \Delta t}(x)\|_2$) decreases at least like $y = x^{0.6}$.

to use inverse problem algorithms to perform parameters' estimation. This may involve a lot of evaluations of the direct problem: knowing (B, S, n) , compute $h(x, t)$. The computation time may be too expensive. This is the justification to build a metamodel (or surrogate model) which is an approximation of the PDE solver which is much faster to compute.

2.3. Final direct problem

With the previous considerations, the forward mapping provides, given B , S and n , the result of the numerical solver at wall-touch, using $n_x = 301$ points for the space discretization. This means that the output is a vector of \mathbb{R}^{301} which corresponds to an approximated height profile. The metamodel and inversions are performed for fixed n , as it is assumed that physicists can provide a precise value for n , but the methodology can be applied for any value of n . Note also that the model (1) varies smoothly with n for the values involved in the applications ($n \sim 1$). Thus the ultimate goal is to estimate B and S given height profile(s) of a fluid in the cavity.

3. Metamodel

A standard procedure for constructing a metamodel is the use of *Polynomial Chaos Expansion* (PCE), which consists in a polynomial approximation. They are often used for uncertainty quantification Le Maître and Knio (2010) or sensitivity analysis Sudret (2015). In order to reduce the dimension of the problem (which is currently $n_x = 301$), we combine this method with a *Principal Component Analysis* (PCA).

3.1. Polynomial chaos expansion (PCE)

We start by describing the PCE procedure for some bounded random vector X of \mathbb{R}^d (in our case $X = (B, S) \in \mathbb{R}^2$) and a computational model $\mathcal{M} : \mathbb{R}^d \rightarrow \mathbb{R}^m$.

We are interested in the random vector $Y = \mathcal{M}(X)$ (in our case, $m = 301$ and $Y \in \mathbb{R}^{301}$ is the height profile at wall-touch). We begin this description for the case $m = 1$ in order to simplify the presentation (section 3.1.1 and first § of section 3.1.2); then we describe the full case with $m \geq 1$ (last § of section 3.1.2). Our goal is to approximate Y by a formula of the type:

$$Y = \sum_{\alpha \in \Lambda} \psi_{\alpha}(X) \quad (9)$$

where $(\psi_{\alpha})_{\alpha \in \Lambda}$ are polynomials. It is assumed that Y has a finite variance, which is reasonable for us since (B, S) lives in a bounded domain and we expect the mapping: $(B, S) \mapsto h$ to be smooth. We also assume that the coordinates of X are independent.

3.1.1. General construction

In this section, we assume that $m = 1$. Let us define f_{X_i} the marginal distribution of the i^{th} component of X . We use it to define an inner product for functions u, v defined on the support S_i of X_i (we recall X belongs to a bounded domain):

$$\langle u, v \rangle_i = \int_{S_i} u(z)v(z)f_{X_i}(z)dz. \quad (10)$$

Using this inner product as a scalar product, we define the orthogonality as usual. Then, classic algebra procedures as Gram-Schmidt allows us to construct a family of orthogonal polynomials $(P_k^i)_{k \in \mathbb{N}}$ which depends on f_{X_i} and is not trivial in general. Still in some particular cases, a known polynomial sequence is recovered. In our case (uniform distribution), we recover the Legendre polynomials. For more examples of known families, see Sudret (2015), Xiu and Karniadakis (2002). Note that originally, the methodology has been introduced with Hermite polynomials. For other functions, we should talk about generalized PCE.

For now, we have constructed families of polynomials in one variable (one family for each component of X). To construct polynomials of the whole X vector, we will use products of univariate polynomials (which makes sense as the components of X are independent). Formally, we introduce multi-indices $\alpha \in \mathbb{N}^d$ as $\alpha = (\alpha_1, \dots, \alpha_d)$ and define:

$$\forall x \in \mathbb{R}^d, \psi_{\alpha}(x) = \prod_{i=1}^d P_{\alpha_i}^i(x_i). \quad (11)$$

In this framework, it can be proven that we can write (see, e.g., Le Maître and Knio (2010)):

$$Y = \sum_{\alpha \in \mathbb{N}^d} c_{\alpha} \psi_{\alpha}(X), \quad (12)$$

where the c_{α} are real and need to be determined.

3.1.2. Implementation considerations

Standardized entries. In fact, the Legendre polynomials (as well as other known families) correspond to a precise distribution (Xiu and Karniadakis (2002)). When the input X does not correspond to one of these known distributions, some methods exist to determine the corresponding family (see Sudret (2015) for references), but the standard procedure consists in transforming X into a new variable \tilde{X} that enters in a known case. In the case of uniform distributions, the standard distribution is the uniform distribution over $[-1, 1]$. However, $B \in [0.5, 250]$ and $S \in [0.05, 120]$. Thus we must change the (B, S) coordinates into (\tilde{B}, \tilde{S}) using the formula :

$$\tilde{B} = \frac{B - 125.25}{125.25}, \quad (13)$$

$$\tilde{S} = \frac{S - 60.025}{60.025}. \quad (14)$$

Truncation order. In practice, we cannot determine an infinite number of coefficients and one has to choose which polynomials to take. For this, let us define the degree of a multivariate polynomial ψ_α by $\sum_{i=1}^d \alpha_i$ (the sum of the degrees of the univariate polynomials defining ψ_α). Usually, polynomials with high degrees are associated with high order of interactions between the inputs, which are generally limited Le Maître and Knio (2010), Sudret (2015). That is the reason why generally, the truncation is done by selecting polynomials of degree lower than a threshold β , usually between 3 and 5.

Thus, once an order of truncation β has been determined, we can rewrite the problem of (12) as:

$$Y \simeq \sum_{q=1}^l c_q \psi_q(X). \quad (15)$$

where we have reordered the polynomials for clarity of notation. Note that l is finite, it depends on the order of truncation β , but l and β are different.

Determination of coefficients. There exist multiple techniques to compute the coefficients of (15). A first distinction is made between *intrusive* and *non-intrusive* methods. The intrusive methods such as Galerkin projection are based on the resolution of modified problems (i.e., not the evaluation of \mathcal{M} itself) which require the design of specific solvers, see Le Maître and Knio (2010). More recently, non-intrusive methods have risen, based only on evaluations of \mathcal{M} and statistical tools. A popular solution is to treat the problem as a least-square minimization problem Migliorati and Nobile (2015), Hadigol and Doostan (2018), Sudret (2015). Given a set of samples $(X^{(1)}, \dots, X^{(r)})$ with their evaluations $(Y^{(1)}, \dots, Y^{(r)})$, we reduce the problem to:

$$\min_{c \in \mathbb{R}^l} \sum_{j=1}^r \left(Y^{(j)} - \sum_{q=1}^l c_q \psi_q(X^{(j)}) \right)^2. \quad (16)$$

More details can be found in Migliorati and Nobile (2015), Hadigol and Doostan (2018) and Sudret (2015).

Multivariate output. (case $m \geq 1$). The last aspect remaining to treat is the fact that in our case, the output is a vector and not a scalar. It seems that in most of the published articles of the literature, the components of the output are all treated separately. This means that we decompose $\mathcal{M}(X) = (\mathcal{M}(X)_1, \dots, \mathcal{M}(X)_m)$ and perform a different PCE for each $\mathcal{M}(X)_i$, resulting in m different computations of parameters. See, e.g., Sudret (2015), Garcia-Cabrejo and Valocchi (2014) and Sun et al. (2020).

3.2. Principal component analysis (PCA)

We hereby give a brief review of the PCA. More details can be found in Jolliffe (2002). In this section, we want to study the random vector $Y \in \mathbb{R}^m$, the mapping \mathcal{M} is completely forgotten. We start by defining $\varphi^0 \in \mathbb{R}^m$ as:

$$\varphi^0 = \arg \max_{\varphi \in \mathbb{R}^m} \text{Var}(\langle \varphi, Y \rangle). \quad (17)$$

We define :

$$\alpha^0 = \langle \varphi^0, Y \rangle. \quad (18)$$

Then α^0 is called the first Principal Component (PC) of Y and φ^0 is its direction. For $1 \leq k \leq m - 1$, we recursively define the k^{th} PC in a similar manner:

$$\varphi^k = \arg \max_{\alpha^0, \dots, \alpha^{k-1}, \langle \varphi, Y \rangle \text{ uncorrelated}} \text{Var}(\langle \varphi, Y \rangle), \quad (19)$$

and

$$\alpha^k = \langle \varphi^k, Y \rangle. \quad (20)$$

With these variables we introduce the matrix notation:

$$\alpha = \varphi Y, \quad (21)$$

where α is the column vector of the α_k and φ is the squared matrix whose lines are the φ^k . One can show that in fact φ is invertible. It follows that we can write $Y = \varphi^{-1} \alpha$, so that the study of α is equivalent to the study of Y . However, α is defined so that most of its variations are contained in its first few components. This allows to reduce the dimension of the problem by performing a truncation on the first PCs:

$$Y \approx \varphi^{-1} \begin{pmatrix} \alpha^0 \\ \vdots \\ \alpha^p \\ \bar{\alpha}^{p+1} \\ \vdots \\ \bar{\alpha}^{m-1} \end{pmatrix}, \quad (22)$$

where $\bar{\alpha}^k = \mathbb{E}[\alpha^k]$ and $p \in \llbracket 1, m - 1 \rrbracket$.

In our case we do not have access to the theoretical distribution of Y . As done in practice Jolliffe (2002), we will thus use a data set which is supposedly a good sampling of Y and use sample variances and expectations to compute the PCs.

3.3. Final surrogate via PCE - PCA coupling

We now go back to the PCE. Until now, the metamodel is given by:

$$S(X) = (\Phi^0(X), \dots, \Phi^{m-1}(X)) \approx \mathcal{M}(X), \quad (23)$$

where Φ^k is the result of the PCE performed on the mapping $X \mapsto \mathcal{M}(X)_k = Y_k$. We replace these m different PCEs performed on the components of Y by PCEs performed on the first PCs. More precisely, we assume that the $p + 1$ first PCs account for most of the variance of Y . Then for $0 \leq k \leq p$, we denote by θ^k the result of the PCE performed on the mapping $X \mapsto \alpha^k(X)$ (by virtue of (21), if Y is viewed as a function of X then α^k can also be viewed as such). We use it for our final metamodel:

$$\hat{S}(X) = \varphi^{-1} \begin{pmatrix} \theta^0(X) \\ \vdots \\ \theta^p(X) \\ \bar{\alpha}^{p+1} \\ \vdots \\ \bar{\alpha}^{m-1} \end{pmatrix} \approx \mathcal{M}(X). \quad (24)$$

We recall that φ and the $\bar{\alpha}^k$ are deterministic quantities precomputed during the PCA step.

Such a combination between PCA and PCE is not common in the literature. Up to the authors' knowledge it has been first used by Blatman and Sudret (2013) and more recently in Hawchar et al. (2017).

4. Results

Of note, in this section, we work with $n = 1$. However, the entire methodology and codes can be used with other values of n , e.g., between 0.2 and 1.2. Moreover as mentioned in paragraph 2.3, the present lubrication model varies smoothly for the values of n considered here ($n \sim 1$). It also turns out that the experimental pastes studied in the last subsection are such that $n = 1$ Vigneaux et al. (2023).

4.1. Metamodel performances

In order to compute the coefficients of the metamodel, a sampling grid in the (B, S) domain has to be established. The exact forward mapping is then evaluated for each couple of the grid. We will work with a small regular grid of 400 couples (20 different values of B and 20 values of S) and a huge regular grid of 6084 couples (78 by 78). Note that the couples which are the longest to be evaluated seem to be the same for all values of n , which means that we can use the existing computations to estimate the duration of the computation of each solution, so that the evaluation of a new dataset can be efficiently parallelized. In practice, the small regular grid can be computed in five hours using seven processors.

Let us now define the precision of a metamodel. Apart from our two regular grids, a validation set of approximately 6000 couples sampled uniformly at random on the (B, S) domain has been precomputed. Given a metamodel $\tilde{\mathcal{M}}$,

Table 1

Different statistics of the errors of reconstruction for different metamodels, where β is the order of truncation for the PCE.

Data set	β	PCA	median	3 rd quantile	max
78x78	4	no	1	1.8	16.8
		yes	1	1.8	16.8
	15	no	0.018	0.027	0.59
		yes	0.018	0.027	0.59
	30	no	0.0011	0.002	0.082
		yes	0.0018	0.0024	0.082
20x20	4	no	1.1	1.9	15.8
		yes	1.1	1.9	15.8
	15	no	0.021	0.032	1.13
		yes	0.021	0.032	1.13

we evaluate it on all the couples of the validation set and compare them to the real outputs $\mathcal{M}(B, S)$. For each couple (B, S) of the validation set, we define the *reconstruction error* $\|\mathcal{M}(B, S) - \tilde{\mathcal{M}}(B, S)\|_2$. Some statistics over the validation set for different parameters of the metamodel are presented in the table 1. We comment them below.

Multiple orders of truncation for the PCE have been tested, from 4 to 30. As expected, the higher the order is, the more precise the metamodel. From order 4 to 6, the error is divided by 3. From 10 to 12 it is divided by 2. At order 30, for the biggest grid, there is approximately 3% of error for most couples of the validation set. There is however a limit to it since there is a limited number of samples, so the system becomes undetermined for a degree high enough. This happens for the smallest grid, which cannot be associated to an order higher than 15. Another practical limit comes from the computation time of the coefficients. While for small orders like 4 or 5, the coefficients are estimated in a few minutes, it can take multiple days to train for order 30.

To combine PCA and PCE, one has to determine a number of principal components (PC) to keep. For instance if one uses only 3 PCs (i.e., $p = 2$ following the notation of the previous section), then the quality of the metamodel reaches a plateau after order 10. Using 10 PCs (i.e., $p = 9$), the precision is almost not affected even at order 30, so that is what we will use. Note that using the PCA with 10 PCs, we have to perform 10 one-dimensional PCEs. If we did not use the PCA, we would have to perform $n_x = 301$ PCEs. So the use of the PCA divides the computation time by 30.

We point out the fact that no matter the parameters of the metamodel, there are always a few couples which lead to a significant error of reconstruction. Even the most precise version has a maximal error of 10% which can be problematic for an inversion procedure. However these extreme cases happen very infrequently and almost only close to the boundary of the (B, S) domain, for small values of B and generally also small values of S . Since the domain has been chosen so that for the applications, the values should be quite far from the boundary, we may expect the error to be under the 3rd quantile.

Until now the focus has been on the precision of the prediction of the metamodel. However, let us recall the reason why a metamodel is needed in the first place is that an inversion procedure will typically require hundreds of evaluations of the model, so that it needs to be evaluated very fast. The metamodels presented above are all a lot faster to evaluate than the real model, but they are not equal. While being slightly more precise, the PCE of order 30 without PCA requires the evaluation of 301 bivariate polynomials of degree 30. In comparison, the PCE of order 15 with PCA only requires 10 polynomials of order 15 and a matrix multiplication. In practice, the latter is three times faster than the first one.

In the figure 3, we present typical reconstructions of the PDE solution by the metamodel approach trained with the 20 x 20 data set, using the PCE of order 15 with PCA. Three representative (B, S) couples are chosen and the associated h profiles given by the PDE solver and by the metamodel are superposed. We observe a very good adequacy of both types of profiles.

Considering all of the above, we will now use the PCE-PCA with $\beta = 15$ (following the notation of the previous section) and $p = 9$, trained on the smallest grid. This provides a precise metamodel which can be evaluated very quickly and which can be trained in a day or two at most (counting the dataset evaluation) on a domestic laptop.

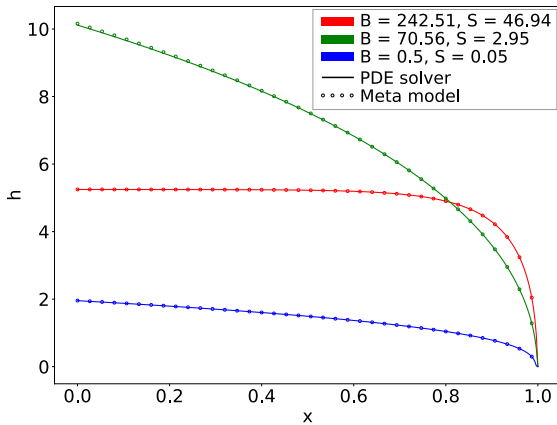


Figure 3: Comparison of the results from the PDE direct solver (solid line) and from the metamodel (circle markers), for three sets of (B, S) parameters (colors).

4.2. Parameters' estimation on synthetic data

The purpose of the metamodel is to be used for parameters' estimation. As a first step we will test it on synthetic data, in the sense that we will use the profiles of the validation set (termed as "real" in the following) and try to retrieve the values of B and S , using our metamodel.

In addition to the real profiles $h(B, S)$, we create noisy profiles out of them. As field data are expected to be available up to a precision of roughly 5% (see next section), we will try 2%, 5%, and 10% of noise intensity. More precisely, we sample $h_{noised}(B, S) = h(B, S) + \varepsilon$ where $\varepsilon \sim \mathcal{N}(0, \alpha h(B, S))$

Table 2

Summary statistics of the errors (eq. (25)) of parameters' estimation.

Noise	median	3 rd quantile	max	var
0%	0.00045	0.00088	0.0299	7.46e-06
2%	0.016	0.043	1.21	0.0276
5%	0.035	0.097	3.07	0.064
10%	0.067	0.18	5.03	0.202

and $\alpha = 0.02, 0.05$ or 0.1 . All in all, for each (B, S) couple, we have at our disposal $h(B, S)$ (the real one) and 3 noisy profiles with respectively 2%, 5%, and 10% noise intensity. We will do so for 500 couples of the original validation set.

The parameters' estimation is performed by the Nelder-Mead algorithm, with a maximum of 400 iterations, see Nelder and Mead (1965) for details on the algorithm. The error of the estimation is defined by the Euclidean distance between the real (B, S) couple and the estimated one. The results are summed up in the table 2. The error displayed is the relative error of the estimated couples, i.e.,

$$err = \left\| \left(\frac{B_{real} - B_{estim}}{B_{real}}, \frac{S_{real} - S_{estim}}{S_{real}} \right) \right\|_2. \quad (25)$$

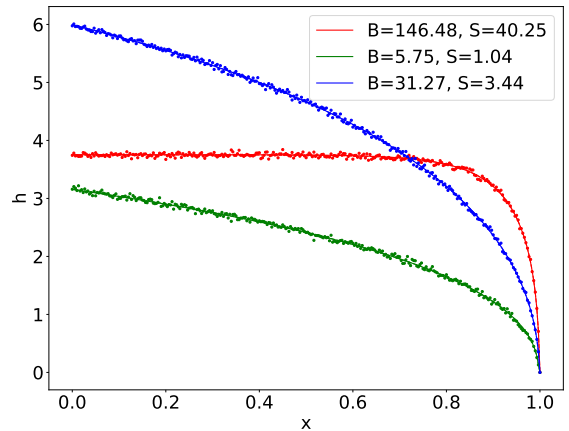


Figure 4: Comparison between a real height profile (solid line), its noisy version (circle) and the profile determined by the Nelder-Mead algorithm (dotted line). The noisy profiles are created using 2% of noise. The three colors correspond to three different (B, S) couples randomly chosen. Note that at this level of zoom the line and the dotted line are superimposed, so only one is visible.

For the non-noisy couples, the estimation is almost exact and for 2% of noise, there is generally less than 5% of error. The situation for 5% of noise is a little worse, with roughly 10% of error in the estimation. Note that these noisy profiles are extremely chaotic compared with what we would expect from experimental data. Still, the profiles corresponding to the couples determined by the algorithm are very close to the real profiles as displayed on the figures 4 and 5. If

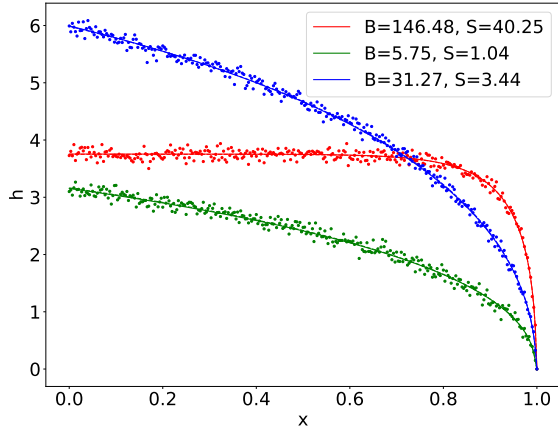


Figure 5: Comparison between a real height profile (solid line), its noisy version (circle) and the profile determined by the Nelder-Mead algorithm (dotted line). The noisy profiles are created using 5% of noise. The three colors correspond to three different (B, S) used in the figure 4. Note that at this level of zoom the line and the dotted line are superimposed, so only one is visible.

the h profiles have 10% of noise, practitioners need to be cautious because the estimation of (B, S) can diverge more significantly than for the previous noise intensities, even though real data would be expected to be less chaotic so the figure 7 (in the Appendix) should be thought of as a worst-case scenario.

4.3. Parameters' estimation on experimental data

In this section, we apply the current algorithm to the experimental data measured in the lab presented in Vigneaux et al. (2023). In this article, four pastes are used to perform four fillings of an empty box – a reduced model in the lab for CPB experiment, with pastes coming from the field. For each experiment the snapshot of the profile of h at wall-touch is obtained (see, e.g., figure 16 of Vigneaux et al. (2023)). This gives four curves $x \mapsto h(x)$ that we can use to perform a (B, S) parameters' estimation.

The results are presented in figure 6. As a first comment, we can note that the experimental data do exhibit a sort of noise whose amplitude is of the same order as in the virtual noise 2% - 5% used in section 4.2. The noise in the experiments is not significantly associated to the image processing but is essentially due to the very "thick" rheological behavior of the pastes (including mounding described below). The parameters values estimated by the metamodel are given in table 3.

It is important to note that (B, S) values were estimated in Vigneaux et al. (2023) with two distinct techniques. Namely one estimation with the fitting of a Bingham constitutive law, and the other with a creep shear experiment. Of note, the estimation of B in the lab is not trivial due to the use of real material as encountered in the field, for which very precise rheometric measurements is a complicated task. The

Table 3

Parameters' estimation with h profiles coming from lab data of Vigneaux et al. (2023). "#" stands for the Paste number. "exp" stands for the estimation done physically in the lab (with two techniques for B). "meta" stands for the estimation obtained with the present metamodel. "var" stands for the percentage of variation between Vigneaux et al. (2023) and present estimation with the metamodel. See main text for details.

#	B : exp	meta	% var	S : exp	meta	% var
1	[43;58]	73	69; 26	0.22	0.05	-77
2	[102;122]	176	73; 44	0.28	0.05	-82
3	[74;98]	137	85; 40	0.28	2.2	686
4	[68;93]	120	76; 29	0.26	0.05	-81

illustration of this can be seen in the significant variability of B shown for the two techniques in the second column of Tab. 3. Another difficulty is the fact that the experiments may present 3D mounding effect (see pastes 1, 2 and 4 in figure 6, around $x = 0.1$) which cannot be captured by the current 2D model (and not 3D) used here. In the present study, this mounding effect translates in a "bump" shape perturbation for x close to 0.1 which is equivalent to a noise on the curve of $h(x)$. This may challenge the inversion procedure which tries to fit the PDE model (without mounding) to the experimental curve.

It is also worth to mention that the lab experiment was such that S is very small due to a very small slope of the experimental device (in operational CPB context, one usually encounters slightly bigger slopes and thus bigger S , as mentioned in section 2.1). This implies that the numerical test for the inverse problem is in a challenging part of the (B, S) parameters' space because:

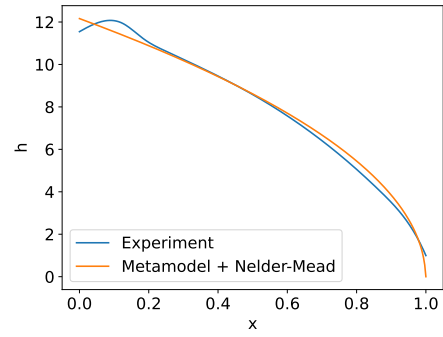
- (i) the smallest grid has been used for training, so the metamodel has been trained with very few values close to the boundary of the (B, S) domain (the two smallest values of S used for training are 0.05 and roughly 6, nothing in between), as a result it can be expected that the metamodel has only a limited precision in this very extreme range of S values;
- (ii) a close inspection of the solutions $x \mapsto h(x)$ for different values of (B, S) shows that for very small S (particularly $S < 1$), only a slight change in the value of S results in a significantly different solution of the PDE, so that both training the metamodel and solving the inverse problem become far more challenging in that area.

All the above reasons explain why this particular test is difficult. As well as the significant percentage of variation seen in the Tab. 3 between the (B, S) values of Vigneaux et al. (2023) and the values estimated by the present Metamodel+inversion procedure.

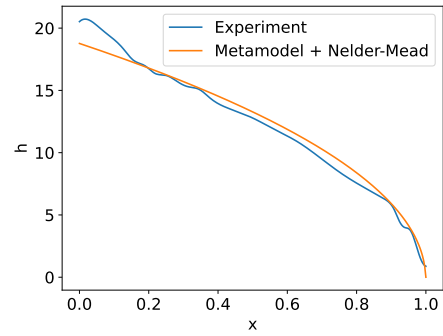
This said, it should be noted that the curves obtained by the metamodel are very well fitted with the experimental curves. It should also be noted that the inversion procedure

is very fast compared to an inversion using a resolution of the PDE. So, given the noise that can be encountered with CPB field materials and the fact that their typical (B, S) live in the bulk (and not at the boundaries) of the parameters' space of the metamodel (giving more accuracy for exploring couples that minimize the discrepancy between the curve of the model and the curve of the experiment), we believe that this metamodel-inversion procedure can be one of the tools to make a first estimation of the rheology of CPB experiments, based on the curve $x \mapsto h(x)$ at wall-touch.

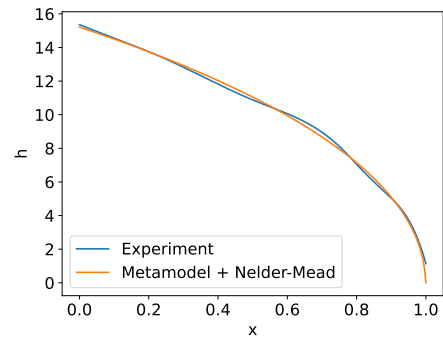
For this purpose, we deliver on the Zenodo open repository Zenodo (2013) the codes and metamodel data Berger and Vigneaux (2023) so that other teams having wall-touch snapshots of $h(x)$ can test the current methodology with their own data.



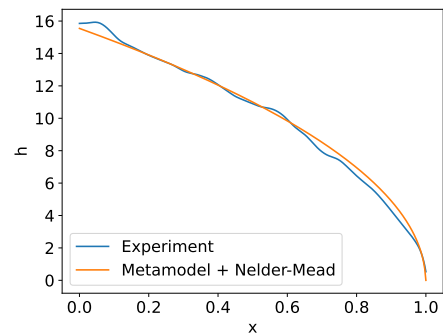
(a) paste 1



(b) paste 2



(c) paste 3



(d) paste 4

Figure 6: Fitting via the parameters' estimation procedure using four different real data sets from Vigneaux et al. (2023). For each paste are displayed in blue the experimental profile $h(x)$ (non-dimensional variables, see section 2.1) and in orange the curve associated to the (B, S) couple estimated by our procedure.

5. Summary and discussion

Based on a partial differential equation (PDE) model derived from a lubrication approximation, we have designed a metamodel approximating this PDE. The metamodel is constructed using a combination of polynomial chaos expansion (PCE) and principal component analysis (PCA). We have extensively tested different combinations of PCE and PCA features, resulting in a metamodel that represents a good compromise between speed and accuracy. As a result, given the two model parameters (B, S), the solutions of the PDE and the metamodel are essentially superimposed, while the computation of the metamodel is much faster. Next, we tested this metamodel for parameters' estimation on synthetic data, including noisy data. It is demonstrated, using statistically relevant samples, that with the typical noise encountered in typical CPB applications, the inversion procedure leads to good parameter estimations. The solutions of the inverse problem are such that the estimate of (B, S) is very good, as is the fit of the height profiles (data that can be obtained from a laboratory snapshot). Finally, we also tested this inversion procedure on a small sample of four available experimental data, in the worst-case scenario, i.e., with a low-slope configuration that lies at the boundary of the parameters' space for CPB (and thus also for the metamodel) with respect to S . The inversion procedure naturally struggles to estimate these (B, S) parameters. Given the high variability of B values obtained in Vigneaux et al. (2023), an average B error of 53% can be considered quite encouraging for such rough pastes and stiff numerical configuration.

In addition, given the good statistical results obtained on the synthetic data, it is expected that with laboratory experiments conducted on CPB configurations mimicking the field, i.e., with $S \sim 10$, inversion with the metamodel can be a valuable tool for performing (B, S) parameters' estimation. For testing purposes, we are providing the data and metamodel codes Berger and Vigneaux (2023) so that other teams can test them on their laboratory data. Not only the ready-to-use metamodel, but also the code to recalculate this metamodel with other parameters, are also provided in the repository, so that another training set of (B, S) and the corresponding metamodel can be computed offline in a few days with a domestic laptop, providing a metamodel specialized in the (B, S) range of a specific type of CPB applications. The code is written in Python and is well-documented so that a minimal investment is required to do so.

Future research directions would include a quantitative study of the influence of the ϕ angle (involved in S), as well as a more systematic study of general slope variations due to layers already deposited at the bottom. It is common practice in CPB to carry out several injections on layers of cemented paste that have already been deposited Mizani et al. (2013).

A. Numerical solver

A.1. Numerical computation of $h(t, 0)$

As stated in section 2.2, the numerical computation of $h(t, 0)$ is not straightforward. The time being fixed, let's write $h_1 = h(t, \Delta x)$ (known) and $h_0 = h(t, 0)$ (unknown). A downwind scheme for $\partial h / \partial x$ and the boundary condition $q(0) = 1$ together with the equation (1) lead to the following problem on h_0 :

$$1 = \tilde{\delta} \frac{n}{(n+1)(2n+1)} Y_d(h_0)^{1+1/n} \times \left| S - \frac{h_1 - h_0}{\Delta x} \right|^{1/n} ((2n+1)h_0 - nY_d(h_0)) \quad (26)$$

with

$$\tilde{\delta} = \text{sgn} \left(S - \frac{h_1 - h_0}{\Delta x} \right), \quad (27)$$

and

$$Y_d(h_0) = \max \left(h_0 - \frac{B}{|S - \frac{h_1 - h_0}{\Delta x}|}, 0 \right). \quad (28)$$

This problem is highly non-linear. However, it is constant equal to 0 whenever $Y_d(h_0) = 0$. On the other part of the real line, it can be checked that the function of h_0 defined by (26) is actually strictly increasing and continuous, implying the uniqueness of the solution of our problem. Because of the power law involved in (26), an external solver is required to numerically solve the problem. In order to accelerate its resolution, we provide to the solver the point after which $Y_d > 0$ (so that it does not get stuck in a constant region). Using (28) and $h_0 \geq 0$, we derive the formula:

$$h_0 > \frac{h_1 - S\Delta x}{2} + \sqrt{\left(\frac{h_1 - S\Delta x}{2} \right)^2 + B\Delta x}. \quad (29)$$

Note that in the special case $n = 1$, the problem (26) is equivalent to finding the root of a polynomial of degree 7. However, in practice, it is not faster than using the methodology presented above.

A.2. Numerical stability condition

We develop the expression (1) of the model, so as to obtain explicitly an advection-diffusion form. Denoting $V(x)$ the transport coefficient and $D(x)$ the diffusion coefficient, (1) is equivalent to:

$$\frac{\partial}{\partial t} h(x, t) + V(x) \frac{\partial}{\partial x} h(x, t) - D(x) \frac{\partial^2}{\partial x^2} h(x, t) = 0 \quad (30)$$

with $\delta = \text{sgn}(S - h_x)$,

$$V(x) = \delta Y^{1/n} |S - h_x|^{1/n} h, \quad (31)$$

and

$$D(x) = \frac{-1}{(1+n)(1+2n)} Y^{1/n} |S - h_x|^{1/n-1} \times \left(2nh \frac{B}{|S - h_x|} + (1+n)h^2 + 2n^2 \frac{B^2}{(S - h_x)^2} \right). \quad (32)$$

At each time iteration, as mentioned in the main text, the time step is determined as:

$$\Delta t = \min \left(\frac{\Delta x}{2 \max_x(V(x))}, C_d \frac{(\Delta x)^2}{\max_x(D(x))} \right) \quad (33)$$

where (the classical) $C_d = 0.5$ ensures stability for most simulations. One can lower C_d , e.g. $C_d = 0.05$ to stabilize the simulation if needed. Note that for the current paper, where the solutions are not computed after the time of wall-touch, $C_d = 0.5$ leads to stable simulations for all studied parameters (B, S).

B. Noisy synthetic profiles

The supplementary figure, mentioned in the main text, concerning the study of noisy profiles with 10% noise.

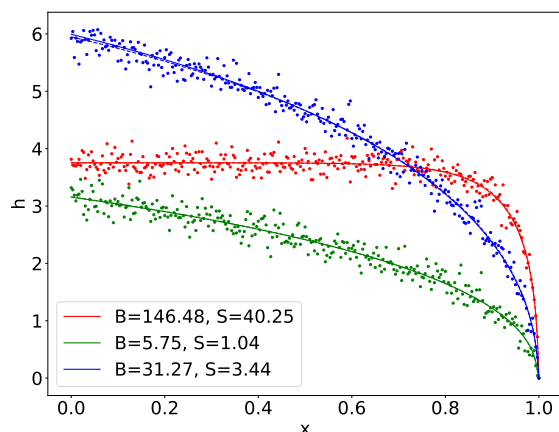


Figure 7: Comparison between a real height profile (solid line), its noisy version (circle) and the profile determined by the Nelder-Mead algorithm (dotted line). The noisy profiles are created using 10% of noise. The three colors correspond to three different (B, S) used in the figure 4.

Acknowledgements

We would like to extend our warmest thanks to Ian Frigaard and Yajian Shao for their fruitful discussions on this work.

This study used components of the SciPy, NumPy, Scikit-learn, Chaospy, Numpy and Matplotlib Python libraries – we thank the respective authors for making their code free and open source.

We gratefully acknowledge support from the PSMN (Pôle Scientifique de Modélisation Numérique) of the ENS de Lyon for the computing resources. This research has been conducted with financial support from the French National Research Agency (ANR) through the research project VPFlows, Grant number: ANR-20-CE46-0006.

CRedit authorship contribution statement

Clément Berger: Conceptualization, Methodology, Software, Writing. **David Coulette:** Data Curation, Software. **Paul Vigneaux:** Conceptualization, Methodology, Software, Writing, Funding.

References

- Azam, S. and Li, Q. (2010). Tailings Dam Failures: A Review of the Last One Hundred Years. *Geotechnical News (Canada USA Mexico)*, 28(4):50–53. Section: Waste Geotechnics.
- Balmforth, N. J., Craster, R. V., Rust, A. C., and Sassi, R. (2006). Viscoplastic flow over an inclined surface. *Journal of Non-Newtonian Fluid Mechanics*, 139(1-2):103–127.
- Berger, C. and Vigneaux, P. (2023). Supplementary code for "A metamodel for confined yield stress flows and parameters' estimation" <https://doi.org/10.5281/zenodo.8377205>. *Zenodo*, page 8377205.
- Blatman, G. and Sudret, B. (2013). Sparse polynomial chaos expansions of vector-valued response quantities. In *Safety, Reliability, Risk and Life-cycle Performance of Structures and Infrastructures*, pages 3245–3252. CRC Press/Balkema.
- Coussot, P., Proust, S., and Ancey, C. (1996). Rheological interpretation of deposits of yield stress fluids. *Journal of Non-Newtonian Fluid Mechanics*, 66(1):55–70.
- Garcia-Cabrejo, O. and Valocchi, A. (2014). Global sensitivity analysis for multivariate output using polynomial chaos expansion. *Reliability Engineering and System Safety*, 126:25–36.
- Hadigol, M. and Doostan, A. (2018). Least squares polynomial chaos expansion: A review of sampling strategies. *Computer Methods in Applied Mechanics and Engineering*, 332:382–407.
- Hawchar, L., Soueidy, C.-P. E., and Schoefs, F. (2017). Principal component analysis and polynomial chaos expansion for time-variant reliability problems. *Reliability Engineering and System Safety*, 167:406–416.
- Hogg, A. J. and Matson, G. P. (2009). Slumps of viscoplastic fluids on slopes. *Journal of Non-Newtonian Fluid Mechanics*, 158(1):101–112.
- Huang, X. and Garcia, M. H. (1998). A Herschel-Bulkley model for mud flow down a slope. *Journal of Fluid Mechanics*, 374:305–333.
- Jolliffe, I. T. (2002). *Principal Component Analysis*. Springer Series in Statistics. Springer, 2 edition.
- Keller, E. A. (2008). *Introduction to environmental geology*. Pearson Prentice Hall, 4th edition.
- Landriault, D. (2006). They Said "It Will Never Work" - 25 Years of Paste Backfill 1981 - 2006. In *Paste 2006: Ninth International Seminar on Paste and Thickened Tailings, 2006 3-7 April*. R.J. Jewell, S. Lawson, P. Newman (eds), pages 277–292, Limerick, Ireland. Australian Centre for Geomechanics.
- Le Maître, O. P. and Knio, O. M. (2010). *Spectral Methods for Uncertainty Quantification, With Applications to Computational Fluid Dynamics*. Scientific Computation. Springer Netherlands.
- LeVeque, R. J. (2004). *Finite Volume Methods for Hyperbolic Problems*. Cambridge University Press.
- Liu, K. F. and Mei, C. C. (1989). Slow spreading of a sheet of Bingham fluid on an inclined plane. *Journal of Fluid Mechanics*, 207:505–529.
- Liu, Y., Balmforth, N. J., Hormozi, S., and Hewitt, D. R. (2016). Two-dimensional viscoplastic dambreaks. *Journal of Non-Newtonian Fluid Mechanics*, 238:65–79.
- Migliorati, G. and Nobile, F. (2015). Analysis of discrete least squares on multivariate polynomial spaces with evaluations at low-discrepancy point sets. *Journal of Complexity*, 31(4):517–542.
- Mizani, S., He, X., and Simms, P. (2013). Application of lubrication theory to modeling stack geometry of high density mine tailings. *Journal of Non-Newtonian Fluid Mechanics*, 198:59–70.
- Nelder, J. A. and Mead, R. (1965). A Simplex Method for Function Minimization. *The Computer Journal*, 7(4):308–313.
- Roussel, N. and Coussot, P. (2005). "Fifty-cent rheometer" for yield stress measurements: From slump to spreading flow. *Journal of Rheology*, 49(3):705–718.

- Sudret, B. (2015). Polynomial chaos expansions and stochastic finite element methods. In *Risk and Reliability in Geotechnical Engineering*, pages 265–300. CRC Press.
- Sun, X., Choi, Y. Y., and Choi, J.-I. (2020). Global sensitivity analysis for multivariate outputs using polynomial chaos-based surrogate models. *Applied Mathematical Modelling*, 82:867–887.
- UNCED (1992). Agenda 21: program of action from the United Nations organization. Technical report, United Nations Conference on Environment and Development (UNCED), Rio de Janeiro, Brazil. §11.13, §13.15, §17.28.
- Vigneaux, P., Shao, Y., and Frigaard, I. A. (2023). Confined yield stress lubrication flows for cement paste backfill in underground stopes <https://doi.org/10.1016/j.cemconres.2022.107038>. *Cement and Concrete Research*, 164:107038.
- Xiu, D. and Karniadakis, G. E. (2002). The Wiener-Askey polynomial chaos for stochastic differential equations. *SIAM Journal on Scientific Computing*, 24(2):619–644.
- Yilmaz, E. and Fall, M. (2017). *Paste tailings management*. Springer.
- Zenodo (2013). European Organization For Nuclear Research and OpenAIRE.